How to cite: *Angew. Chem. Int. Ed.* **2025**, *64*, e202420220
doi.org/10.1002/anie.202420220

Nitrogen Fixation

Chemocatalytic Conversion of Dinitrogen to Ammonia Mediated by a Tungsten Complex

Anna-Marlene Vogt, Tobias A. Engesser, Jan Krahmer, Niels Michaelis, Mareike Pfeil, Jannik Junge, Christian Näther, Nicolas Le Poul,* and Felix Tuczek**

Dedicated to Professor Rüdiger Beckhaus on the occasion of his retirement

Abstract: Whereas molybdenum dinitrogen complexes have played a major role as catalytic model systems of nitrogenase, corresponding tungsten complexes were in most cases found to be catalytically inactive. Herein, we present a modified pentadentate tetrapodal (pentaPod) phosphine ligand in which two dimethylphosphine groups of the pentaPod^{Me} (P5^{Me}) ligand have been replaced with phospholanes (Pln). The derived molybdenum complex [Mo(N$_2$)P5^{Pln}] generates 22 and the analogous tungsten complex [W(N$_2$)P5^{Pln}] 7 equivalents of NH$_3$ from N$_2$ in the presence of 180 equivalents of SmI$_2$(THF)$_2$/H$_2$O, rendering the latter the first tungsten complex chemocatalytically converting N$_2$ to NH$_3$. In contrast, the tungsten complex [W(N$_2$)P5^{Me}] generates ammonia from N$_2$ only in a slightly overstoichiometric fashion. The reasons for these reactivity differences are investigated with the help of spectroscopic and electrochemical methods.

Introduction

The conversion of dinitrogen to ammonia with transition metal complexes has been of continued interest during the last decades.[1–11] Molybdenum systems catalytically mediating the nitrogen reduction reaction (N$_2$RR) have played an important role in this research area, starting in 2003 with the complex [Mo(N$_2$)(N(HIPTN)$_3$)] (HIPT = hexa-*iso*-propylterphenyl) developed by Schrock et al.[12,13] However, first N$_2$RR investigations have already been presented much earlier by the groups of Chatt and Hidai in the 1960s on [M(N$_2$)$_2$(diphos)$_2$] (M=Mo, W) complexes.[8,14–18] This work also prominently included low-valent tungsten systems. Chatt et al., e.g., reported that the reaction of the tungsten–dinitrogen complex *cis*-[W(N$_2$)$_2$(PMe$_2$Ph)$_4$] with an excess amount of H$_2$SO$_4$ in MeOH at room temperature almost quantitatively generates ammonia (1.98 equiv./W), whereas the molybdenum analogue affords only a small amount of ammonia (0.64 equiv./Mo).[19,14] This was ascribed to the weaker electron-donating ability of molybdenum.[8,19,20] Nevertheless, ammonia generation from W-dinitrogen complexes has always been stoichiometric or lower,[2,4,8,14,21–26] and no tungsten system chemocatalytically converting N$_2$ to NH$_3$, as observed for molybdenum complexes, has been reported to date. Instead, it appears that the hydrogen evolution reaction (HER), which is also mediated by tungsten-based systems,[1,27–31] outcompetes N$_2$RR in the presence of SmI$_2$(THF)$_2$/H$_2$O. Thus, using 180 equivalents of this *proton coupled electron transfer* (PCET) reagent, 80 equivalents of H$_2$ were detected with the tungsten complex [W(N$_2$)P5^{Me}] (**3**, Scheme 1).[28,32,33] This conforms to an isolated tungsten-substituted nitrogenase which also turned out to be inactive towards N$_2$RR, but active for HER.[34] Notably, the tungsten analog of Schrock's complex, [W(N$_2$)(N(HIPTN)$_3$)], has been found to be inactive towards catalytic ammonia formation from N$_2$ as well.[35] This lack of activity was suggested to be due to the challenging conversion of W–NH$_3$ into W–N$_2$.[35] Also regarding other

[*] A.-M. Vogt, Dr. T. A. Engesser, Dr. J. Krahmer, N. Michaelis, Dr. M. Pfeil, Dr. J. Junge, Prof. Dr. C. Näther, Prof. Dr. F. Tuczek
Institut für Anorganische Chemie
Christian-Albrechts-Universität zu Kiel
Max-Eyth-Straße 2, 24118 Kiel, Germany
E-mail: ftuczek@ac.uni-kiel.de
tengesser@ac.uni-kiel.de

Dr. N. Le Poul
Univ. Brest, CNRS, UMR 6521, F 29200 Brest, France
E-mail: nicolas.lepoul@univ-brest.fr

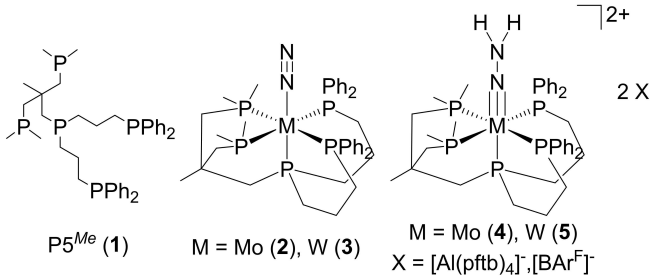

Scheme 1. Molybdenum and tungsten dinitrogen complexes supported by the pentaPod^{Me} ligand (P5^{Me}, **1**). Depending on the acid used in the synthesis of complexes **4** and **5** the anions are X=[Al(pftb)$_4$]$^-$ (tetrakis(perfluoro-tert-butoxy)aluminate) or X=[BAr^F]$^-$ (tetrakis(3,5-bis(trifluoromethyl)phenyl)borate).

aspects of N_2 chemistry, differences in reactivity between molybdenum and analogous tungsten complexes have been evidenced.[36,37] On the other hand, tungsten complexes are more stable than their molybdenum counterparts; therefore, W- rather than Mo-complexes have often been employed in studies aiming at a functionalization of N_2 coordinated to group 6 transition metals.[38–41]

A number of papers on electrochemical NH_3 generation with Chatt-type tungsten and molybdenum complexes have been published since the 1980s.[42,43] In 2022, Peters et al. successfully produced up to 40 equivalents of ammonia by electrocatalysis, using the complex $[W(N_2)_2(dppe)_2]$ (dppe:1,2-bis(diphenylphosphino)ethane).[44] This suggests that, in principle, it should be possible to employ a tungsten catalyst for chemocatalytic N_2RR as well.[44–46] For its lighter homologue molybdenum, our group observed a significant impact of the ligand design on the catalytic activity of Chatt-type complexes. In particular, we found that tridentate and tripodal ligands were ineffective, but using the tetrapodal pentadentate ligand pentaPod^{Me} (P5^{Me}) in $[Mo(N_2)P5^{Me}]$ resulted in catalytic amounts of ammonia (Scheme 1).[47–50] In an attempt to replicate this success with tungsten and to understand the reasons for different catalytic activity of Mo and W, we prepared the analogous tungsten complex $[W(N_2)P5^{Me}]$.[28,32] Similar to Schrock's system, only slightly overstoichiometric amounts of ammonia were observed and the dominant catalytic activity was found to be HER.[28,32] Interestingly, detailed electrochemical investigations indicated only minor differences in M^0/M^I redox potentials,[32,28] and additional theoretical investigations showed no significant differences regarding the thermodynamics of N_2RR and the thermodynamics/kinetics of HER between the two metals.[28]

Pursuing this line of research further, we also investigated the effect of different phosphine residues on the amount of produced ammonia. The coordination behavior of the pentaPod ligand can, for instance, be tuned by replacing the phosphinyl residues by groups with differing donor strength or steric demand (e.g. phospholane groups).[47,51] Accordingly, we herein present the synthesis and characterization of Mo- and W-complexes supported by a modified tetrapodal pentadentate ligand, pentaPod^{Pln} (P5^{Pln}), in which two dimethylphosphine groups of the original pentaPod^{Me} ligand[32,50,52] have been replaced with phospholano groups, as we already did with tridentate and tripodal ligand designs.[47] In the presence of $SmI_2(THF)_2$/H_2O,[33,53,54] the W-complex supported by the P5^{Pln} ligand is (chemo−)catalytically active towards N_2RR, rendering it the first example of a tungsten complex with this property. This is in contrast to the analogous tungsten complex supported by the original P5^{Me} ligand containing dimethylphosphine groups that is catalytically inactive.[32] On the other hand, the catalytic activity of the Mo complex supported by the new P5^{Pln} ligand is almost equal to that of the parent system.[50] The reasons for these differences in reactivity are investigated.

Results and Discussion

Synthesis and characterization of $[M(N_2)P5^{Pln}]$ (M=Mo, W). The synthesis and characterization of the new ligand P5^{Pln} (**6**) and its complexes follows that of the original pentaPod^{Me} ligand (P5^{Me}, **1**). The dinitrogen complexes $[Mo(N_2)P5^{Me}]$ (**2**) and $[W(N_2)P5^{Me}]$ (**3**) derived from **1** as well as the hydrazido(*2−*) complexes $[Mo(NNH_2)P5^{Me}]^{2+}$ (**4**) and $[W(NNH_2)P5^{Me}]^{2+}$ (**5**) have previously been described and discussed in detail (Scheme 1).[32,49]

Analogous to the synthesis of the ligand P5^{Me} (**1**),[49] P5^{Pln} (**6**) was prepared by using **Li-Pln** as P nucleophile instead of $LiPMe_2 \cdot \frac{1}{2}\ Et_2O$ in the last step (Scheme 2, cf. Figure S1–S5).[47,51]

The preparation of the molybdenum and tungsten complexes **7–10**, bearing the pentaPod^{Pln} ligand, is similar to that applied for the synthesis of the dinitrogen complexes **2** and **3** coordinated by pentaPod^{Me} (Scheme 3, cf. Figure S6, S7).[32,49,50] Under nitrogen atmosphere, the Mo^{III} (**7**) and W^{III} (**8**) complexes were reduced by sodium amalgam resulting in the formation of $Mo^0(N_2)$ (**9**) and $W^0(N_2)$ (**10**), respectively, supported by P5^{Pln} (Scheme 3, cf. Figure S8–S30).

Single crystals of $[W(N_2)P5^{Pln}]$ (**10**) were obtained from a THF solution layered with methanol. Single crystal X-ray diffraction (SC-XRD) analysis shows an octahedral complex with pentaphosphine environment (Figure 1, cf. Supporting Information crystal data Table S1, Table S2). The W-P_{ax} bond length (2.3918(11) Å) is shorter than the average W-P_{eq} bond lengths (2.4389 Å, SI). This finding is consistent

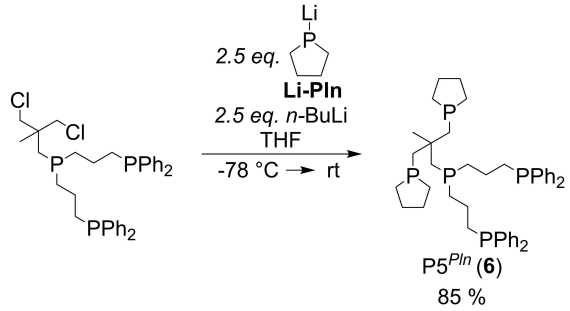

Scheme 2. Synthesis of the pentadentate tetrapodal phosphine (pentaPod) ligand with phospholane (Pln) groups P5^{Pln} (**6**).

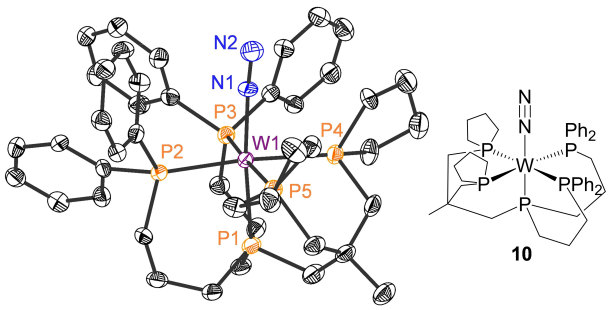

Figure 1. Crystal structure (ORTEP plot) of $[W(N_2)P5^{Pln}]$ (**10**) with labeling and displacement ellipsoids drawn at the 50% probability level. Hydrogen atoms are omitted for clarity.

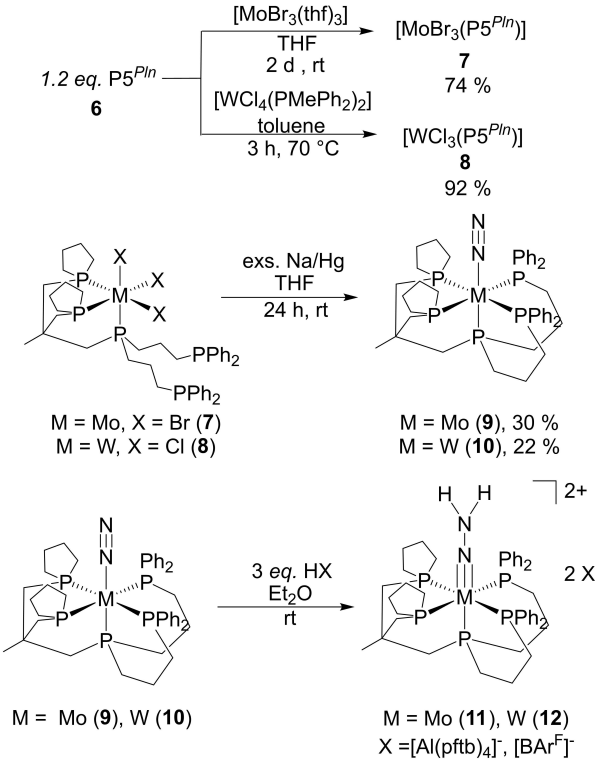

Scheme 3. Synthesis of molybdenum and tungsten complexes supported by pentaPod^{Pln} (P5^{Pln}, **6**); exs: excess.

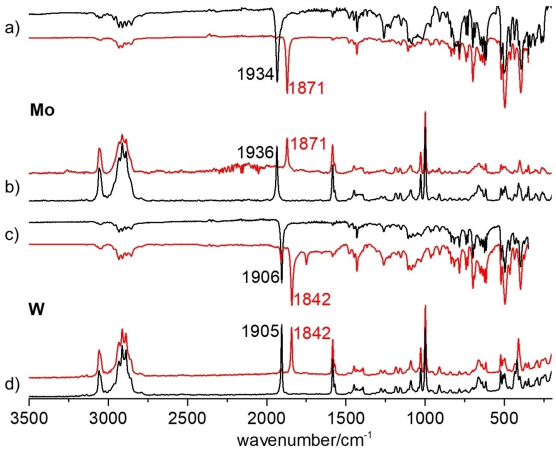

Figure 2. IR(ATR) and Raman spectra measured of (a, b) **9** (black), **^{15}N-9** (red) and (c, d) **10** and **^{15}N-10** (red) showing the band of the N–N stretching vibration.

Table 1: N–N stretching vibrations (ν_{NN}/cm^{-1}) of dinitrogen complexes with pentapodal ligands [M(N$_2$)(P5^R)] (R=Me, M=Mo (**2**), M=W (**3**); R=Pln, M=Mo (**9**), M=W (**10**)) and their ^{15}N isotope labelled analogues.[32,49]

M	P5^{Me}	P5^{Pln}
Mo	1929 (**2**)	1934 (**9**)
	1868 (**^{15}N-2**)	1871 (**^{15}N-9**)
W	1901 (**3**)	1906 (**10**)
	1840 (**^{15}N-3**)	1842 (**^{15}N-10**)

with the results obtained for **3**. Due to the higher steric demand of the phospholane donors of the newly synthesized pentaPod^{Pln} ligand **6** compared to the dimethylphosphine groups of **1**, the W-P$_{eq}$ and W-P$_{ax}$ bond lengths of **10** are slightly longer (about $1\cdot10^{-3}$ Å) than in **3**.[32] Whereas the W–N$_\alpha$ bond lengths (2.020(3) Å for **3**, 2.021(4) Å for **10**) are equal within the error limits, a slight elongation of the N–N bond is observed for **10** (N-N = 1.084(5) Å for **3**; 1.102(6) Å for **10**, cf. Table S2). Apart from this important parameter, the single-crystal data of [W(N$_2$)P5^{Pln}] (**10**) and the tungsten complex **3** bearing pentaPod^{Me} indicate only very small differences.[32]

The N≡N bond weakening in the case of a coordinated N$_2$ ligand and, thus, its activation are reflected by a lowering of the wavenumber of the N–N valence stretching vibration.[55,56] Solid-state IR (ATR) and Raman spectra show a N–N stretching vibration for [Mo(N$_2$)P5^{Pln}] (**9**) at 1934 cm^{-1} and for [W(N$_2$)P5^{Pln}] (**10**) at 1906 cm^{-1} which in both cases is 5 cm^{-1} higher than observed for the analogous complex supported by the pentaPod^{Me} ligand (Figure 2 and Table 1).

Thus, the N$_2$ ligands in complexes **9** and **10** supported by pentaPod^{Pln} are slightly less activated compared to the previously published, analogous pentaPod^{Me} complexes **2** and **3**. Moreover, for both ligand systems the N–N stretch of the W complex (**3** or **10**) is 28 cm^{-1} lower than that of the Mo congener (**2** or **9**), suggesting a higher degree of activation in the respective W system. Nevertheless, complex **3** did not exhibit any chemocatalytic activity for N$_2$RR, in contrast to **2**.[32] The impact of the changed substitution in the ligand (R=Me vs. R=Pln) on the catalytic activity of **9** and **10** is considered below. The reduction of the Mo^{III} (**7**) and, respectively, W^{III} (**8**) precursor was also carried out under ^{15}N$_2$ atmosphere, providing [Mo(^{15}N$_2$)P5^{Pln}] (**^{15}N-9**) and [W(^{15}N$_2$)P5^{Pln}] (**^{15}N-10**) with N–N stretching vibrations appearing at 1871 cm^{-1} (**^{15}N-9**) and 1842 cm^{-1} (**^{15}N-10**). Based on the isotopic shift and in agreement with the literature it was possible to identify the M-N$_2$ stretching vibration at 411 cm^{-1} for [Mo(N$_2$)P5^{Pln}] (**9**) (403 cm^{-1} for **^{15}N$_2$-9**) and 420 cm^{-1} for [W(N$_2$)P5^{Pln}] (**10**) (411 cm^{-1} for **^{15}N$_2$-10**) in the Raman spectra (cf. Figure S31).[56]

In order to obtain information about the donor properties of the ligand in solution, NMR spectroscopy was employed. Notably, the ^{31}P{^{1}H} NMR spectrum of the newly obtained pentaPod^{Pln} ligand **6** exhibits a low-field shift of P^{Pln} nuclei compared to the P^{Me} nuclei of pentaPod^{Me} (**1**) (cf. Figure S70, S71).[49] This suggests that the P^{Pln} groups containing C$_4$ rings are less electron-donating than the P^{Me} groups of **1**.[28,32,49] In analogy to previous studies of complexes exhibiting a pentaphosphine ligation, especially with pentaPod^{Me} (**1**), an AA′XX′M coupling pattern was expected[49] but, instead, an AA′BB′M spin system pattern was obtained in the ^{31}P{^{1}H} NMR spectra of **9** (cf. Figure S14) and **10** (Figure 3). A low-field shift of the P^{Pln} signals was observed for [Mo(N$_2$)P5^{Pln})] (**9**) and [W(N$_2$)P5^{Pln}] (**10**) as well. Regarding the chemical shifts of the tungsten

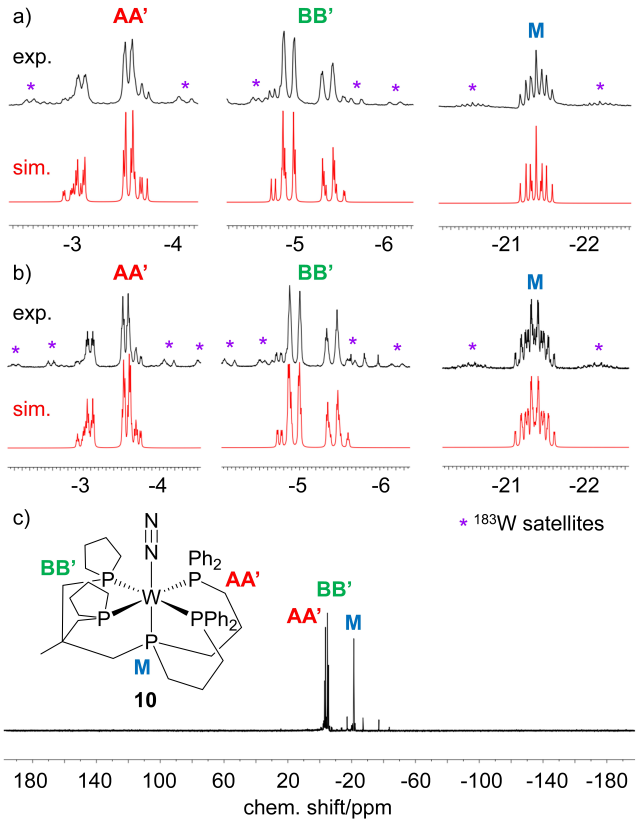

Figure 3. Experimental $^{31}P\{^{1}H\}$ NMR spectra of [W(N$_2$)P5^{Pln}] (**10**) (a, c) and ^{15}**N-10** (b) in benzene-d_6 at 300 K, compared with the simulation (red). * = tungsten satellites.

complex **10** with $P^{AA'} = -3.42$ ppm and $P^{BB'} = -5.20$ ppm, it is still possible to distinguish between the AA′ and BB′ signal (Figure 3), but in case of the molybdenum complex **9** the AA′ and BB′ subspectra with $P^{AA'} = 25.33$ ppm and $P^{BB'} = 25.20$ ppm overlap too strongly (cf. Figure S14), so a simulation was not possible. Therefore, we focused on the tungsten-based systems **10** and **12** for more detailed NMR-spectroscopic investigations and analysis of the coupling constants (cf. Table S3).

Importantly, measuring the ^{15}N-labelled complexes allows a detailed NMR-spectroscopic analysis of the M-N$_2$ unit in the [M(N$_2$)P5^R] complexes. In this context, we note that $^1J(^{15}N_\alpha, ^{15}N_\beta)$ is lower in ^{15}**N-10** (6.0 Hz) than in ^{15}**N-3** (7.4 Hz).[50] This reflects a weakening of the N–N bond, in agreement with the X-ray structure determination (see above). This effect is also visible in the molybdenum congeners with a decrease from 6.9 Hz (^{15}**N-2**)[49] to 6.0 Hz (^{15}**N-9**) (cf. Table S5, S6). In case of tungsten, the ^{183}W isotope (14.3 %) can give additional information about the bonding situation and allows comparison of the metal-mediated effect of the pentaPod ligand on the activated N$_2$.[57–59] The substitution of PMe$_2$ by phospholane in particular affects the $^1J(^{31}P_{XX'/BB'}, ^{183}W)$ coupling constant which decreases from 269 to 264 Hz (cf. Table S4), reflecting a weakening of the corresponding W–P bonds. By contrast, $^1J(^{31}P_{AA'}, ^{183}W)$ and $^1J(^{31}P_M, ^{183}W)$ remain constant within ≈2 Hz.

Relevant information can also be derived from $^1J(^{183}W, ^{15}N_\alpha)$. Whereas for the pentaPod^{Me} complex ^{15}**N-3** a value of 45 Hz is obtained (cf. Table S6), determination of this coupling constant is difficult for the pentaPod^{Pln} complex ^{15}**N-10** due to its low solubility. Direct comparison of the two spectra, however, suggests that $^1J(^{183}W, ^{15}N_\alpha)$ is decreased for ^{15}**N-10** with respect to ^{15}**N-3**, reflecting a weakening of the metal-N bond in the former complex with respect to the latter (cf. Figure S30). This hypothesis as well as its implication on the N–N bond strength will be investigated in more detail with the help of quantum-chemical calculations in a future study.

In summary, NMR parameters thus indicate weaker N–N bonds and possibly a weaker metal-N-bond in the pentaPod^{Pln} complexes as compared to their pentaPod^{Me} counterparts. In particular, the N$_2$-ligand in [W(N$_2$)P5^{Pln}] complex **10** is more activated than in its catalytically inactive analog [W(N$_2$)P5^{Me}] (**3**).

Synthesis and characterization of [M(NNH$_2$)P5^{Pln}]$^{2+}$ with M=Mo (11), W (12). Hereafter, protonation of the new dinitrogen complexes **9** and **10** to their hydrazido(*2−*) derivatives was investigated. Previous studies in our group revealed that [Mo(NNH$_2$)P5^{Me}]$^{2+}$ (**4**) is capable of N$_2$-to-NH$_3$ reduction in solution using SmI$_2$(THF)$_2$ (180 equiv.s) and water (180 equiv.s) as PCET reagent.[50] Specifically, **4** afforded 26.14±0.32 equiv.s of NH$_3$, almost the same value as observed for the parent N$_2$ complex **2**.[50] Similar to the procedure applied for the synthesis of **4** (Mo)[50] and **5** (W),[32] the hydrazido(*2−*) complexes [Mo(NNH$_2$)P5^{Pln}]X$_2$ (**11**) and [W(NNH$_2$)P5^{Pln}]X$_2$ (**12**) (with X=[BAr^F]$^-$, tetrakis-(3,5-bis(trifluoromethyl)phenyl)borate or X=[Al(pftb)$_4$]$^-$, tetrakis(perfluoro-tert-butoxy)aluminate) were generated by adding 3 equiv.s of Brookhart's acid HBAr^F ([H(OEt$_2$)$_2$][BAr^F]) or [H(OEt$_2$)$_2$][Al(pftb)$_4$] to the dinitrogen complexes **9** and **10** (Scheme 3, cf. Figure S44, S45, S51, S59, S60, S62). Smaller amounts of acid did not lead to the desired products. Retention of the pentaphosphine environment is evident from the $^{31}P\{^{1}H\}$ NMR spectra of **11**-[Al(pftb)$_4$]$_2$ and **12**-[Al(pftb)$_4$]$_2$ exhibiting the corresponding AA′BB′M coupling patterns. Overall, the signals for the **11**-[Al(pftb)$_4$]$_2$ and **12**-[Al(pftb)$_4$]$_2$ are high-field shifted compared to the dinitrogen complexes **9** and **10**, which is consistent with the observations made for hydrazido(*2−*) complexes **4** and **5**. The most pronounced high-field shift is observed for the M-signal due to the *trans*-influence of the π-donating NNH$_2$-ligand and the corresponding weakening of the M-P$_M$ bond.[50] As with the corresponding Mo- and W-dinitrogen complexes, a remarkable low-field shift is observed for the BB′ (respectively XX' signals) of the tungsten (**5**→**12**: △ = 27.2 ppm cf. Figure S62 and Table S3) and molybdenum NNH$_2$-complexes (**4**→**11**: △ = 25.3 ppm; cf. Figure S44)[32,49,50] whereas the chemical shifts of the AA′ nuclei are very similar for the P^{Pln} based systems **11** and **12** compared to the P^{Me} systems **4** and **5**.[32,49,50] Interestingly, regardless of the coordinated pentaPod ligand, the shift of the P$_M$ signal appears to be almost identical in the molybdenum (P$_M$ = −48.6 ppm for **4** and P$_M$ = −47.5 ppm for **11**) and tungsten

complexes ($P_M = -33.09$ ppm for **5** and $P_M = -31.95$ ppm for **12**). Apparently, the equatorial donors P^{Me} or P^{Pln} do not have a significant impact on the chemical shift of P_M.[32,50]

For the analysis of the bonding situation in the NNH_2 ligand, which is the most relevant part of the molecule regarding nitrogen fixation, ^{31}P- and ^{15}N NMR-spectroscopic investigations of the ^{15}N-labeled hydrazido(*2−*) complexes **^{15}N-11**-$[Al(pftb)_4]_2$ and **^{15}N-12**-$[Al(pftb)_4]_2$ were performed (cf. Figure S47–S49; Figure S62, S66–S68). The obtained coupling constants, however, did not reveal notable differences to the corresponding molybdenum and tungsten NNH_2-complexes **4** and **5** supported by the original pentaPod^{Me} ligand **1** (cf. Table S7; Table S8).[32,49]

Chemocatalytic N_2-reduction to ammonia. The newly obtained Mo and W dinitrogen complexes **9** and **10** were examined for their catalytic activity under the same conditions as their counterparts **2** and **3** supported by the pentaPod^{Me} ligand. For this purpose, a 0.1 M $SmI_2(THF)_2/H_2O$ (1:1) solution in THF was stirred with the catalyst (**9** or **10**) in a 50 mL Schlenk flask at room temperature under a nitrogen atmosphere. The chosen concentrations correspond to 180 equiv.s of $SmI_2(THF)_2/H_2O$ per catalyst.[33] In case of the experiments with molybdenum complex **9** bearing the pentaPod^{Pln} ligand, the amount of the generated ammonia was determined by the indophenol method as soon as the reaction solution turned yellow, usually after 10 h. Based on the small differences in activation (see above), we expected similar catalytic results for **9** compared to **2**. In fact, under identical conditions, **9** was able to produce 22.16 ± 0.34 equiv.s of ammonia as a catalyst. This is somewhat less than generated by $[Mo(N_2)P5^{Me}]$ (**2**), which produces 25.73 ± 0.37 equiv.s, but can be traced back to the slightly lower activation of **9** as compared to **2** (see above) (Table 2). Then, the tungsten dinitrogen complex $[W(N_2)P5^{Pln}]$ (**10**) was studied under the same (chemo−)catalytic conditions. After stirring for about 10 h and work-up of the reaction solution, 6.79 ± 0.39 equiv.s ammonia could be detected. This result, which at first was surprising in view of the close similarity to the catalytically inactive tungsten complex $[W(N_2)P5^{Me}]$ (**3**, see above), renders $[W(N_2)P5^{Pln}]$ (**10**) the first tungsten (chemo−)catalyst capable of converting N_2 to NH_3.

Table 2: Results of the N_2 to NH_3 conversion under chemocatalytic conditions (180 equiv.s $SmI_2(THF)_2/H_2O$, 1 atm N_2) with pentaPod^R complexes $[M(N_2)P5^R]$ and *in situ* generated $[M(NNH_2)P5^R]^{2+}$ complexes (M=Mo, R=Me (**2**), Pln (**9**); M=W, R=Me (**3**), Pln (**10**)).[50,32]

$$N_2 + 6\,H_2O + 6\,SmI_2(thf)_2 \xrightarrow[\text{THF, rt, 10 h}]{\text{2 µmol catalyst}} NH_3$$

complex (catalyst)	$P5^R$	equiv.s NH_3/M
$[Mo(N_2)P5^R]$	$P5^{Me}$ (**2**)	25.73 ± 0.37[50]
	$P5^{Pln}$ (**9**)	22.16 ± 0.34
$[Mo(NNH_2)P5^R]^{2+}$	$P5^{Me}$ (**4**)	26.14 ± 0.32[50]
	$P5^{Pln}$ (**11**)	22.71 ± 0.62
$[W(N_2)P5^R]$	$P5^{Me}$ (**3**)	2.75 ± 0.23[32]
	$P5^{Pln}$ (**10**)	6.79 ± 0.39
$[W(NNH_2)P5^R]^{2+}$	$P5^{Me}$ (**5**)	1.91 ± 0.16
	$P5^{Pln}$ (**12**)	7.34 ± 0.37

Besides the N_2 complexes (**2**, **3**, **9** and **10**, see Table 2), the corresponding hydrazido(*2−*) complexes bearing $P5^{Pln}$ were applied as catalysts for N_2-to-NH_3 reduction under the same conditions (see above). In analogy to our previous studies[32,50] hydrazido(*2−*) complexes **11** and **12** were generated in situ and subsequently added to the prepared $SmI_2(THF)_2/H_2O$ solution in THF. Under the given conditions, these catalysis experiments afforded 22.71 ± 0.62 equiv.s ammonia with $[Mo(NNH_2)P5^{Pln}]^{2+}$ (**11**) respectively 7.34 ± 0.37 equiv.s with $[W(NNH_2)P5^{Pln}]^{2+}$ (**12**) (Table 2). The detected equiv.s of ammonia produced by hydrazido(*2−*) complexes **11** and **12** correspond, within error limits, to the expected amount of ammonia detected with their corresponding N_2 complexes **9** and **10**.

Based on the structural and spectroscopic data, the emergence of catalytic activity in **10** can be traced back to replacement of the PMe_2 groups, contained in the original pentaPod ligand, with phospholane groups, resulting in a more activated N_2 ligand (see above).

Electrochemistry. The unprecedented catalytic activity of the tungsten complex **10** prompted us to investigate its electrochemical properties in relation to its molybdenum congener **9** and its (catalytically inactive) tungsten analog **3**, respectively. In a recent article,[32] we showed by cyclic voltammetry (CV) studies that the Mo- and W–N_2 complexes **2** and **3** supported by the classic pentaPod^{Me} ligand **1** can be reversibly oxidized in THF/$NaBPh_4$ (20 mM) through single electron transfer processes at *ca.* −1.15 V vs. Fc^+/Fc. Here, we present electro-chemical studies of these two complexes (**2** and **3**) as well as the new complexes **9** and **10** in THF/Na[BAr^F] (30 mM) and THF/Li[$Al(pftb)_4$] (30 mM). The Na[BAr^F] and Li[$Al(pftb)_4$] electrolytes were specifically chosen as the weakly coordinating anions $[BAr^F]^-$ and, in particular, $[Al(pftb)_4]^-$ are even more inert from a redox/Brønsted basicity point of view than BPh_4^- (tetraphenylborate).[60–62] Measurement of the four N_2 complexes $[Mo(N_2)P5^{Me}]$ (**2**), $[W(N_2)P5^{Me}]$ (**3**), $[Mo(N_2)P5^{Pln}]$ (**9**) and $[W(N_2)P5^{Pln}]$ (**10**) in THF/Na[BAr^F] (30 mM) showed reversible oxidation processes at −1.17 V (**2**), −1.19 (**3**), −1.18 V (**9**) and −1.19 V (**10**) vs. Fc^+/Fc (Figure S78A,B and S79A,B). The determined values are similar to previous ones found in THF/$NaBPh_4$ (20 mM) for **2** and **3**. However, in contrast to the measurements in $NaBPh_4$, an additional reversible process was found at −1.51 V vs. Fc^+/Fc for $Mo(N_2)$ complexes **2** and **9**, as well as a new reduction peak at −1.44 V and −1.45 V vs. Fc^+/Fc for $W(N_2)$ complexes **3** and **10**, respectively. At this stage, it was not possible to identify the species to which the additional redox waves in the CVs of N_2 complexes **2**, **3**, **9** and **10** belong. Measurements of the corresponding NNH_2 complexes in THF/Na[BAr^F] were not successful since the complexes decomposed immediately under these conditions (see Figure S78C,D, S79C,D). Thus, THF/Li[$Al(pftb)_4$] (30 mM) was employed to further study the electrochemical properties of the complexes. As shown in Figure 4A (blue curve), the W–N_2 complex **3** in THF/Li[$Al(pftb)_4$] (30 mM) displays a reversible system at $E_{1/2}(1) = -1.22$ V vs. Fc^+/Fc (anodic peak potential −1.17 V)

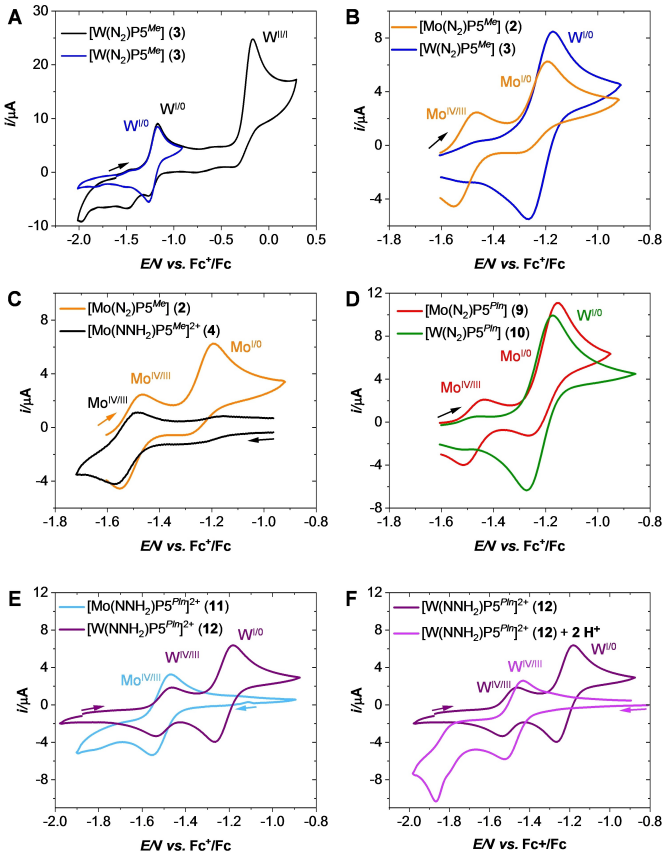

Figure 4. CVs at a glassy carbon working electrode in THF/Li[Al(pftb)$_4$] (30 mM) under argon of A) complex **3** (blue and black) for different potential ranges; B) complexes **2** (orange) and **3** (blue); C) complex **2** (orange) and **4** (black); D) complexes **9** (red) and **10** (green); E) complex **11** (light blue) and complex **12** (purple); F) complex **12** (purple) and complex **12** with two added equivalents of acid ([H(OEt$_2$)$_2$][Al(pftb)$_4$]) (pink). The arrows indicate the initial scanning direction and the starting potential values. Concentration in complex: 1 mM. *E*/V vs. Fc^+/Fc, scan rate $\nu = 0.1$ V/s.

upon oxidation, ascribed to the $W^{I/0}$ couple by analogy with previous studies in THF/$NaBPh_4$.[32] Scan rate (ν) variation shows a linear dependence of anodic and cathodic peak currents i_{pa} and i_{pc} with $\nu^{1/2}$, as expected for a diffusion-controlled process (cf. Figure S72). Scanning towards more positive potential values reveals an irreversible oxidation peak at −0.17 V for $\nu = 0.1$ V/s with high current intensity (Figure 4A, black curve), suggesting the loss of N_2 at the W(II) redox state, as previously observed in THF/$NaBPh_4$.[32] On the back scan, supplementary reduction peaks are detected in the −1.2 V to −2.0 V potential range, due to the new species generated through the irreversible oxidation at −0.17 V. The same experiments were then performed with [Mo(N_2)P5^{Me}] (**2**). In contrast to [W(N_2)P5^{Me}] (**3**) which exhibits one redox wave at −1.22 V *vs.* Fc^+/Fc for the reversible $W^{I/0}$ couple, two redox processes were detected in the −1.6 V to −1.0 V potential range for the molybdenum based system **2** (Figure 4B, orange curve). The first process at $E_{1/2}$ (2) = −1.49 V vs. Fc^+/Fc was found to be reversible whereas the $Mo^{I/0}$ oxidation wave at E_{pa} (1) = −1.17 V displayed irreversibility at $\nu = 0.1$ V/s due to decoordination of N_2 at the Mo(I) state and solvent coordination, as previously derived from IR-spectroelectrochemistry.[32] On the other hand, the process at $E_{1/2}$ (2) = −1.49 V indicates that the $Mo^0(N_2)$ complex **2** converts into a new species. One possible explanation is that protons are released from traces of water present in the electrolyte, partly generating a $Mo^{IV}(NNH_2)^{2+}$ species that can be reversibly reduced into the $Mo^{III}(NNH_2)^+$ complex at −1.49 V (see Scheme 4).

Using Karl Fischer titration (cf. Table S9) the water content of the THF used for the electrochemical studies was determined to 12.7 ppm, which corresponds to approximately 1 mM H_2O in THF. Thus, it approximately equals the concentration of the Mo and W complexes. Formation of the hydrazido(*2−*) species is confirmed by voltammetric study of the chemically synthesized $Mo^{IV}(NNH_2)^{2+}$ penta-Pod^{Me} complex **4**. As shown in Figure 4C, **4** displays a reversible signature at $E_{1/2}$ (2) = −1.49 V; i.e., at exactly the position where the new redox wave of **2** appears.

The direct influence of the water content in the electrolyte solution on the formation of $Mo^{IV}(NNH_2)$ species **4** was further demonstrated by first dissolving [Mo(N_2)P5^{Me}] (**2**) in THF/Li[Al(pftb)$_4$] (30 mM) and hereafter adding 10 µL water to this solution. Directly a decrease of the oxidation peak at −1.17 V for the $Mo^{I/0}$ redox couple was observed.

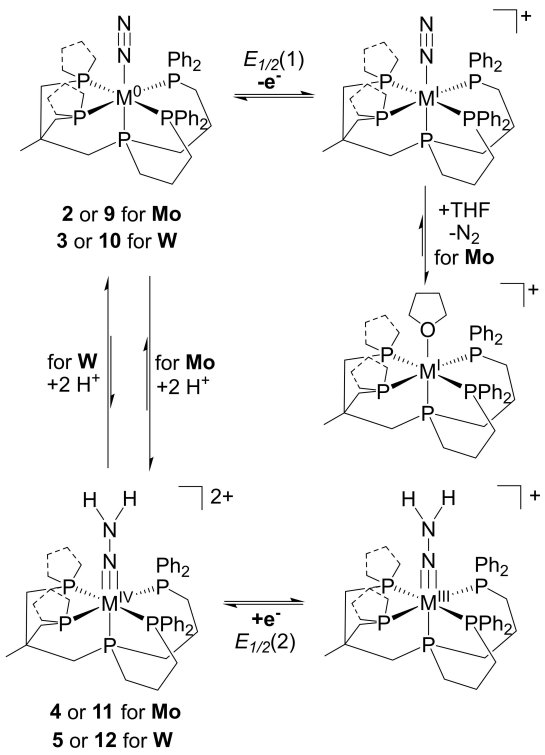

Scheme 4. Electron and proton exchange pathways for investigated complexes according to electrochemical data, showing the difference of basicity between Mo and W species.

Simultaneously, an increase of the reversible redox wave at $E_{1/2}$ (2) = −1.49 V ascribed to the $Mo^{IV}(NNH_2)^{2+}/Mo^{III}(NNH_2)^{+}$ couple was determined. Upon further adding 20 µL of water, the redox wave for the Mo^{IV}/Mo^{III} couple of the $Mo(NNH_2)$ complex **4** did not increase to the same extent as the electrochemical signal of the $Mo(N_2)$ complex decreased, indicating that the N_2 or NNH_2 complex starts to decompose under these conditions (cf. Figure S80).

In order to account for the influence of the phospholano group on the redox properties of the Mo and W dinitrogen complexes, similar experiments were then carried out with the pentaPod^{Pln} complexes **9** and **10**. As shown in Figure 4D (green curve), $W(N_2)$ complex **10** displays the same voltammetric signature with a $W^{I/0}$ oxidation found at $E_{1/2}$ (1) = −1.22 V vs. Fc^{+}/Fc as its pentaPod^{Me} analogue **3**. Likewise, the voltammetric behavior of the $[Mo(N_2)P5^{Pln}]$ complex **9** (red curve in panel D) is qualitatively similar to that of pentaPod^{Me} complex **2** (orange curves in panels in Figure 4B and C), but again different to that of the corresponding $W(N_2)$ complex **10**: whereas the latter exhibits only one (reversible) system at −1.21 V, CV of **9** shows one reversible oxidation at $E_{1/2}$ (2) = −1.47 V and one quasi-reversible process at $E_{1/2}$ (1) = −1.21 V upon oxidation. By analogy with **2**, the two successive systems can be assigned to the $Mo^{IV}(NNH_2)^{2+}/Mo^{III}(NNH_2)^{+}$ and $Mo^{I}(N_2)^{+}/Mo^{0}(N_2)$ redox couples, respectively.

Taken together, the introduction of phospholane in place of two dimethylphosphine groups thus does not appear to significantly modify the redox properties of, both, Mo and W systems, which at some point was unexpected given the lower electron-donating properties of the phospholane compared to methyl phosphine groups.[32] Irrespective of the pentaPod ligand, however, the voltammetric data collected in the THF/Li[Al(pftb)$_4$] electrolyte revealed a marked difference in basicity between the Mo dinitrogen complexes **2** and **9** on one side and their tungsten counterparts **3** and **10** on the other.

Complementary studies were carried out with the Mo-(NNH_2) and W(NNH_2) pentaPod^{Pln} complexes **11** and **12**, respectively. For the Mo complex **11** only one reversible system at −1.47 V corresponding to the $M^{IV}(NNH_2)^{2+}/M^{III}(NNH_2)^{+}$ redox couple was detected (Figure 4E, light blue, and Table 3), similar to the analogous pentaPod^{Me} complex **4** (Figure 4C, black). By contrast, two reversible systems at −1.49 V and −1.22 V vs. Fc^{+}/Fc corresponding to the $W^{IV}(NNH_2)^{2+}/W^{III}(NNH_2)^{+}$ and $W^{I}(N_2)^{+}/W^{0}(N_2)$ redox couples, respectively, were observed for the W-congener **12** (Figure 4E, purple), indicating a partial conversion to the N_2 complex. Similar results were obtained for the analogous W-pentaPod^{Me} NNH_2-complex **5**. Adding two equivalents of acid reprotonates the N_2 complex, and a CV exclusively exhibiting the $W^{IV/III}$ wave of the NNH_2 complex is obtained (Figure 4F, pink, cf. Figure S76, S77B). These data reflect a higher acidity of the W–NNH_2 systems compared to their Mo congeners, which in turn confirms the higher basicity of the Mo- compared with the W-complexes inferred from the measurements of the corresponding dinitrogen systems (Scheme 4).

Further evidence for the different acidities of Mo and W complexes could be obtained by UV/Vis spectroscopy. Notably, the electronic absorption spectra of $[W(N_2)P5^{Pln}]$ (**10**) and $[W(NNH_2)P5^{Pln}]^{2+}$ (**12**) shown in Figure 5 closely resemble those of classic Chatt complexes;[63] similar spectra are obtained for the respective Mo congeners as well as their P5^{Me} analogs (cf. Figure S81).

Regarding the dinitrogen complex(es), the intense bands at 310–320 nm correspond to MLCT transitions into the π* orbitals of N_2 and the broad shoulders at ~400 nm to MLCT transitions into π* orbitals of the phenylphosphine groups.[63] Upon protonation to the NNH_2 complex(es), the absorption

Table 3: Electrochemical data for N_2 and NNH_2 complexes of Mo and W with pentaPod^{Me} (**2–5**) and pentaPod^{Pln} ligands (**9–12**) (1 mM) determined from CV measurements at a glassy carbon electrode in THF/Li[Al(pftb)$_4$] (30 mM) for ν = 0.1 V/s.

	Ligand (L)	Metal	***E*/V vs. $Fc^{+/0}$**	**redox couple**
[M(L)P5^{Me}]	N_2	Mo (**2**)	$E_{pa}(1) = -1.17$[a]	$Mo^{I/0}$
		W (**3**)	$E_{1/2}(1) = -1.22$	$W^{I/0}$
	NNH_2	Mo (**4**)	$E_{1/2}(2) = -1.49$	$Mo^{IV/III}$
		W (**5**)	$E_{1/2}(2) = -1.48$	$W^{IV/III}$
[M(L)P5^{Pln}]	N_2	Mo (**9**)	$E_{1/2}(1) = -1.21$	$Mo^{I/0}$
		W (**10**)	$E_{1/2}(1) = -1.22$	$W^{I/0}$
	NNH_2	Mo (**11**)	$E_{1/2}(2) = -1.47$	$Mo^{IV/III}$
		W (**12**)	$E_{1/2}(2) = -1.49$	$W^{IV/III}$

[a] Irreversible anodic peak.

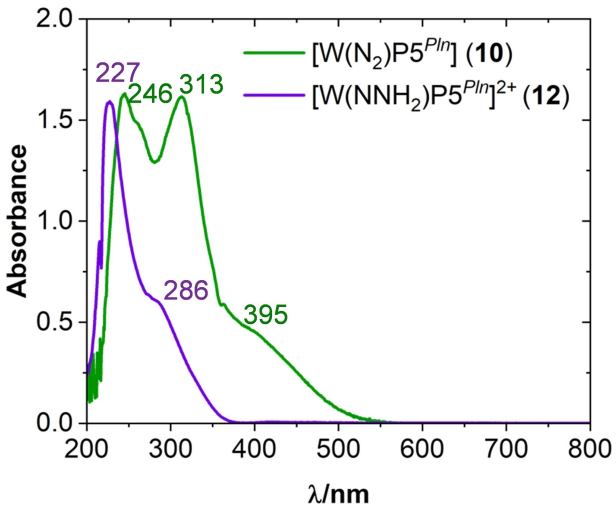

Figure 5. UV/Vis spectra of $[W(N_2)P5^{Pln}]$ (**10**, 0.1 mM) in THF and $[W(NNH_2)P5^{Pln}]^{2+}$ (**12**, 0.1 mM) in CH_3CN.

intensity in the visible region drastically decreases and the absorption edge shifts by over 100 nm into the UV (Figure 5 and Figure S81). This can be exploited to follow the gradual formation of NNH_2 species starting from N_2 complexes in THF/Li[Al(pftb)$_4$] (Figure 6). However, at a concentration of 1 mM of the investigated complexes, the absorbance is too high to measure a UV/Vis spectrum. Therefore and in order to approximately match the conditions of the CV experiments, a concentration of 0.5 mM of the N_2 species (**2**, **3**, **9**, and **10**) in 15 mM Li[Al(pftb)$_4$] was chosen, whereby slight artifacts could not be avoided in the UV/Vis spectra (Figure 6 and S82). However, the electrolyte to complex ratio this way equals 1:30, without drastically changing the ratio of complex concentration to water content in THF (see above).

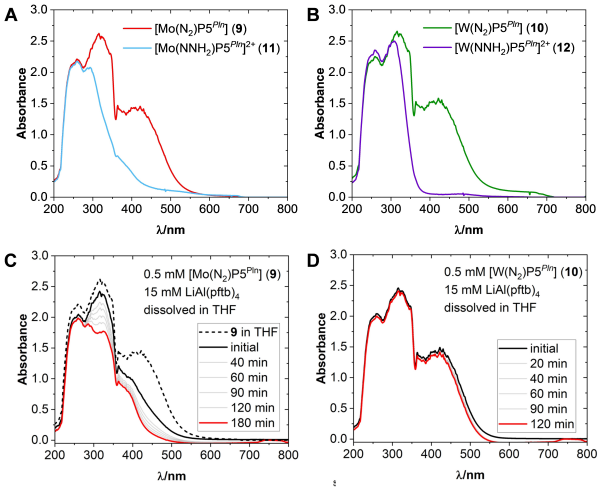

Figure 6. UV/Vis spectra measured in THF of A) $[Mo(N_2)P5^{Pln}]$ (**9**, 0.5 mM) and $[Mo(NNH_2)P5^{Pln}]^{2+}$ (**11**, 0.5 mM); B) $[W(N_2)P5^{Pln}]$ (**10**, 0.5 mM) and $[W(NNH_2)P5^{Pln}]^{2+}$ (**12**, 0.5 mM). UV/Vis spectra under electrochemical conditions (1:30; complex: electrolyte) in THF measured at various time intervals of C) $[Mo(N_2)P5^{Pln}]$ (**9**) dissolved in 15 mM Li[Al(pftb)$_4$] and D) $[W(N_2)P5^{Pln}]$ (**10**) dissolved in 15 mM Li[Al(pftb)$_4$].

UV/Vis spectra of all N_2 and NNH_2 complexes at a concentration of 0.5 mM are quite similar for Mo and W as central atoms as well as $P5^{Me}$ (**1**) and $P5^{Pln}$ (**6**) as supporting ligands (Figure 6A,B and S82A,B), analogous to the spectra recorded at lower concentration (see Figure 5 and S81). Under nearly electrochemical conditions (0.5 mM complex/15 mM Li[Al(pftb)$_4$]), the UV/Vis spectra of the $Mo(N_2)$ complexes **2** and **9** show an intensity decrease in the broad bands at 320 nm and 390 nm after dissolution in the electrolyte (Figure 6C, dashed line and Figure S82C). This process continues over a period of 180 min, and the spectra of the $Mo(N_2)$ complexes **2** and **9** progressively transform into those of the respective $Mo(NNH_2)$ complexes **4** and **11** (Figure 6A and Figure S82A). Importantly, for the UV/Vis spectra of the $W(N_2)$ complexes **3** and **10** in 15 mM Li[Al(pftb)$_4$] no such spectral development is observed, even after more than an hour (Figure 6D and Figure S82 D); i.e., the spectrum measured under almost electrochemical conditions stays unchanged. Therefore, the UV/Vis data support a less basic behavior of the $[W(N_2)P5^{Pln}]$ (**10**) complex and an increased stability under electrochemical conditions compared to $[Mo(N_2)P5^{Pln}]$ (**9**), which slowly reacts to its NNH_2 complex. Notably, this process is not due to an intrinsic acidity of water contained in trace amounts in the solvent, but to reaction of water with the electrolyte, leading to the precipitation of LiOH and the generation of protonated THF which in turn acts as the protonating agent.

Conclusions

In this work, a novel pentadentate tetrapodal phosphine ligand with phospholane donors $P5^{Pln}$ (pentaPod^{Pln}) was presented, thus extending the pentaPod concept beyond the original pentaPod^{Me} system. Molybdenum and tungsten complexes supported by the pentaPod^{Pln} ligand were synthesized and characterized. Investigations of $[Mo(N_2)P5^{Pln}]$ (**9**) as a catalyst provided 22 equivalents of NH_3 using 180 equiv.s of $SmI_2(THF)_2/H_2O$ as PCET reagent. The N–N stretching frequency already indicated that the $Mo^0(N_2)$ complex supported by the pentaPod^{Pln} may be slightly less catalytically active regarding N_2RR than its predecessor $[Mo(N_2)P5^{Me}]$ (**2**) which generated 26 equiv.s of NH_3 under these conditions. More surprising was the observation that the $[W(N_2)P5^{Pln}]$ complex (**10**) gave catalytic amounts of ammonia, rendering it the first chemocatalytically active tungsten complex. By analyzing these complexes via CV in THF and Li[Al(pftb)$_4$] electrolyte no remarkable variance in redox potentials (ca. $E_{1/2}$ (1) ≈ -1.21 V vs. Fc^+/Fc) for the one-electron oxidation of all Mo^0 and $W^0(N_2)$ was found, indicating that this redox process is not specifically perturbed by the nature of the metal (Mo/W) or ligand (pentaPod^{Me} or pentaPod^{Pln}). This also holds for the one-electron reduction processes involving Mo^{IV} and W^{IV} NNH_2 species which occur at ca. $E_{1/2}$ (2) ≈ -1.49 V. Nevertheless, using the supporting electrolyte Li[Al(pftb)$_4$] an unexpected

voltammetric response was observed for the $Mo^0(N_2)$ species which is attributed to acid-base reactions under the applied electrochemical conditions. In the conversion of $Mo^0(N_2)$ to $Mo^{IV}(NNH_2)^{2+}$ observed in the CVs, the protons required for this reaction can be obtained from the water in the THF (notably, the water content of the solvent corresponds to ~1 equiv. of water/complex). Since the formation of hydrazido(*2−*) complex was not observed in the CV data of the tungsten complexes, the $Mo^0(N_2)$ complexes are more basic than their $W^0(N_2)$ analogs, regardless of the ligand used.

The last result points to an important difference in reactivity between molybdenum and tungsten dinitrogen complexes, which may, at least in part, explain the lower catalytic activity of the latter regarding N_2RR with respect to their Mo counterparts. For the Schrock system the missing catalytic activity of the [W(N(HIPTN)$_3$)] system has been attributed to an inability of the W–NH_3 complex to convert to the W–N_2 complex, corresponding to the last step of the reactive cycle (see above).[35] In contrast, our results indicate a reduced basicity of the W–N_2 complexes, impeding their protonation. This would refer to the first step of the reactive cycle, in fact the most critical reaction of N_2-reduction.[64] Although this step in the framework of SmI_2-$(THF)_2/H_2O$ reduction is thought to proceed as part of PCET involving coupled electron/proton transfer to a W(I)–N_2 species,[50] the overall free reaction enthalpy of the latter process also depends on the pK_B value of the N_2 complex; i.e., its protonability.[65,66] These findings thus lead to the surprising conclusion that tungsten dinitrogen complexes such as **3** and **10**, although exhibiting *lower* N–N stretching frequencies than their molybdenum congeners, are in fact *less* activated towards protonation than the latter, in apparent contradiction to a fundamental paradigm of small-molecule activation.[25] It should be mentioned, however, that a similar result has been obtained by investigating adducts of Lewis acids to transition-metal dinitrogen complexes.[67] Specifically, the equilibrium constant for the reaction with $AlMe_3$ turned out to be *higher* for $[Mo(N_2)_2(dppe)_2]$ than for $[W(N_2)_2(dppe)_2]$, reflecting a higher Lewis-basicity of the Mo- as compared to the W-dinitrogen complex.[68] Notably, this experiment probes σ-donation (as opposed to charge distribution), indicating that W is a stronger σ-acceptor than Mo. *Via* σ-donation, however, also charge is transferred from the N_2-ligand to the metal center, thus reducing its Brønsted basicity.

Finally, the emergence of catalytic activity in the tungsten complex $[W(N_2)P5^{Pin}]$ (**10**) as opposed to its catalytically inactive counterpart $[W(N_2)P5^{Me}]$ (**3**) has been investigated. As evidenced by X-ray structure analysis and NMR spectroscopy, **10** exhibits an elongation of the N–N bond with respect to **3**, causing an increased activation of the N_2 ligand as compared to the latter complex. For the corresponding W(IV)-hydrazido(*2−*) complexes **5** and **12**, similar structural or spectroscopic differences could not be evidenced. Nevertheless, the question of whether the increased activation of the N_2-ligand of **10** is the only reason for the catalytic activity of this complex (contrary to the catalytic inactivity of **3**) or whether other (e.g., kinetic) factors at (possibly) other intermediate stages of the Chatt cycle also play a role cannot be answered with certainty at present.

Acknowledgements

The authors gratefully acknowledge the SEA-EU program supported by Agence Nationale de la recherche (ANR-19-GURE-0001), PHC Procope Campus France (46652ZL) and Programm des Projekt bezogenen Personenaustauschs Frankreich (PROCOPE) 2021–2023 (Deutscher Akademischer Austauschdienst) for funding. The authors thank Prof. Ingo Krossing for providing us with $[H(OEt_2)_2][Al(pftb)_4]$ and $Li[Al(pftb)_4]$. Open Access funding enabled and organized by Projekt DEAL.

Conflict of Interest

The authors declare no conflict of interest.

Data Availability Statement

The data that support the findings of this study are available in the supplementary material of this article.

Keywords: ammonia · catalysis · tungsten · cyclic voltammetry · nitrogen fixation

[1] M. J. Chalkley, M. W. Drover, J. C. Peters, *Chem. Rev.* **2020**, *120*, 5582–5636.
[2] N. Stucke, B. M. Flöser, T. Weyrich, F. Tuczek, *Eur. J. Inorg. Chem.* **2018**, *2018*, 1337–1355.
[3] Y. Tanabe, Y. Nishibayashi, *Chem. Soc. Rev.* **2021**, *50*, 5201–5242.
[4] Y. Tanabe, Y. Nishibayashi, *Coord. Chem. Rev.* **2022**, *472*, 214783.
[5] M. Hidai, Y. Mizobe, *Chem. Rev.* **1995**, *95*, 1115–1133.
[6] T. A. Bazhenova, A. E. Shilov, *Chem. Soc. Rev.* **1995**, *144*, 69–145.
[7] R. L. Richards, *Coord. Chem. Rev.* **1996**, *154*, 83–97.
[8] J. Chatt, J. R. Dilworth, R. L. Richards, *Chem. Rev.* **1978**, *78*, 589–625.
[9] R. Hille, *Trends Biochem. Sci.* **2002**, *27*, 360–367.
[10] J. Chatt, G. A. Heath, R. L. Richards, *J. Chem. Soc. Chem. Commun.* **1972**, 1010–1011.
[11] R. A. Henderson, G. J. Leigh, C. J. Pickett, *The Chemistry of Nitrogen Fixation and Models for The Reactions of Nitrogenase*, Elsevier **1983**.
[12] D. V. Yandulov, R. R. Schrock, *Science* **2003**, *301*, 76–78.
[13] R. R. Schrock, *Angew. Chem. Int. Ed.* **2008**, *47*, 5512–5522.
[14] J. Chatt, A. J. Pearmen, R. L. Richards, *Nature* **1975**, *253*, 39–40.
[15] M. Hidai, K. Tominari, Y. Uchida, *J. Am. Chem. Soc.* **1972**, *94*, 110–114.
[16] M. Hidai, *Coord. Chem. Rev.* **1999**, *185–186*, 99–108.
[17] C. J. Pickett, *J. Biol. Inorg. Chem.* **1996**, *1*, 601–606.

[18] R. L. Richards, *Nitrogen fixation - The Chemical-Biochemical-Genetic Interface. Dinitrogen Complexes and their Reactions*, Plenum Press, New York **1983**.
[19] J. Chatt, A. J. Pearman, R. L. Richards, *J. Chem. Soc. Dalton Trans.* **1977**, 1852.
[20] J. Chatt, R. L. Richards, *J. Organomet. Chem.* **1982**, *239*, 65–77.
[21] M. Hidai, Y. Ishii, *Bull. Chem. Soc. Jpn.* **1996**, *69*, 819–831.
[22] C. J. Pickett, K. S. Ryder, J. Talarmin, *Dalton Trans.* **1986**, 1453.
[23] F. Masero, M. A. Perrin, S. Dey, V. Mougel, *Chem. Eur. J.* **2021**, *27*, 3892–3928.
[24] K. Arashiba, K. Sasaki, S. Kuriyama, Y. Miyake, H. Nakanishi, Y. Nishibayashi, *Organometallics* **2012**, *31*, 2035–2041.
[25] C. J. Weiss, A. N. Groves, M. T. Mock, W. G. Dougherty, W. S. Kassel, M. L. Helm, D. L. DuBois, R. M. Bullock, *Dalton Trans.* **2012**, *41*, 4517–4529.
[26] C. J. Weiss, J. D. Egbert, S. Chen, M. L. Helm, R. M. Bullock, M. T. Mock, *Organometallics* **2014**, *33*, 2189–2200.
[27] R. R. Schrock, *Acc. Chem. Res.* **2005**, *38*, 955–962.
[28] J. Junge, T. A. Engesser, F. Tuczek, *Chem. Eur. J.* **2023**, *29*, e202202629.
[29] D. J. Schild, J. C. Peters, *ACS Catal.* **2019**, *9*, 4286–4295.
[30] B. Schluschaß, J. Abbenseth, S. Demeshko, M. Finger, A. Franke, C. Herwig, C. Würtele, I. Ivanovic-Burmazovic, C. Limberg, J. Telser, S. Schneider, *Chem. Sci.* **2019**, *10*, 10275–10282.
[31] O. Einsle, T. A. Engesser, F. Tuczek, *Comprehensive Inorganic Chemistry III. Biological and synthetic nitrogen fixation*, Elsevier **2023**.
[32] J. Junge, S. Froitzheim, T. A. Engesser, J. Krahmer, C. Näther, N. Le Poul, F. Tuczek, *Dalton Trans.* **2022**, *51*, 6166–6176.
[33] Y. Ashida, K. Arashiba, K. Nakajima, Y. Nishibayashi, *Nature* **2019**, *568*, 536–540.
[34] S. Siemann, K. Schneider, M. Oley, A. Müller, *Biochemistry* **2003**, *42*, 3846–3857.
[35] D. V. Yandulov, R. R. Schrock, *Can. J. Chem.* **2005**, *83*, 341–357.
[36] H. K. Wagner, H. Wadepohl, J. Ballmann, *Angew. Chem. Int. Ed.* **2021**, *60*, 25804–25808.
[37] L. Eberle, S. Lindenthal, J. Ballmann, *Inorg. Chem.* **2024**, *63*, 3682–3691.
[38] A. Simonneau, R. Turrel, L. Vendier, M. Etienne, *Angew. Chem. Int. Ed.* **2017**, *56*, 12268–12272.
[39] A. Coffinet, D. Specklin, L. Vendier, M. Etienne, A. Simonneau, *Chem. Eur. J.* **2019**, *25*, 14300–14303.
[40] A. Coffinet, D. Zhang, L. Vendier, S. Bontemps, A. Simonneau, *Dalton Trans.* **2021**, *50*, 5582–5589.
[41] A. Bouammali, A. Coffinet, L. Vendier, A. Simonneau, *Dalton Trans.* **2022**, *51*, 10697–10701.
[42] C. J. Pickett, J. Talarmin, *Nature* **1985**, *317*, 652–653.
[43] J. Y. Becker, S. Avraham, *J. Electroanal. Chem. Interfacial Electrochem.* **1990**, *280*, 119–127.
[44] P. Garrido-Barros, J. Derosa, M. J. Chalkley, J. C. Peters, *Nature* **2022**, *609*, 71–76.
[45] M. J. Chalkley, P. Garrido-Barros, J. C. Peters, *Science* **2020**, *369*, 850–854.
[46] J. C. Peters, *Faraday Discuss.* **2023**, *243*, 450–472.
[47] M. Pfeil, T. A. Engesser, J. Krahmer, C. Näther, F. Tuczek, *Z. Anorg. Allg. Chem.* **2021**, *647*, 1778–1788.
[48] S. Hinrichsen, A.-C. Schnoor, K. Grund, B. Flöser, A. Schlimm, C. Näther, J. Krahmer, F. Tuczek, *Dalton Trans.* **2016**, *45*, 14801–14813.
[49] S. Hinrichsen, A. Kindjajev, S. Adomeit, J. Krahmer, C. Näther, F. Tuczek, *Inorg. Chem.* **2016**, *55*, 8712–8722.
[50] T. A. Engesser, A. Kindjajev, J. Junge, J. Krahmer, F. Tuczek, *Chem. Eur. J.* **2020**, *26*, 14807–14812.
[51] M. Pfeil, T. A. Engesser, A. Koch, J. Junge, J. Krahmer, C. Näther, F. Tuczek, *Eur. J. Inorg. Chem.* **2020**, *2020*, 1437–1448.
[52] J. Junge, T. A. Engesser, J. Krahmer, C. Näther, F. Tuczek, *Z. Anorg. Allg. Chem.* **2021**, *647*, 822–831.
[53] A. Eizawa, K. Arashiba, H. Tanaka, S. Kuriyama, Y. Matsuo, K. Nakajima, K. Yoshizawa, Y. Nishibayashi, *Nat. Commun.* **2017**, *8*, 14874.
[54] Y. Ashida, T. Mizushima, K. Arashiba, A. Egi, H. Tanaka, K. Yoshizawa, Y. Nishibayashi, *Nat. Synth.* **2023**, *2*, 635–644.
[55] F. Studt, F. Tuczek, *J. Comput. Chem.* **2006**, *27*, 1278–1291.
[56] F. Tuczek, K. H. Horn, N. Lehnert, *Coord. Chem. Rev.* **2003**, *245*, 107–120.
[57] E. Carmona, A. Galindo, M. L. Poveda, R. D. Rogers, *Inorg. Chem.* **1985**, *24*, 4033–4039.
[58] S. Donovan-Mtunzi, R. L. Richards, J. Mason, *J. Chem. Soc. Dalton Trans.* **1984**, 469–474.
[59] S. Donovan-Mtunzi, R. L. Richards, J. Mason, *J. Chem. Soc. Dalton Trans.* **1984**, 1329–1332.
[60] I. Krossing, *Chem. Eur. J.* **2001**, *7*, 490–502.
[61] I. M. Riddlestone, A. Kraft, J. Schaefer, I. Krossing, *Angew. Chem. Int. Ed.* **2018**, *57*, 13982–14024.
[62] T. A. Engesser, M. R. Lichtenthaler, M. Schleep, I. Krossing, *Chem. Soc. Rev.* **2016**, *45*, 789–899.
[63] N. Lehnert, F. Tuczek, *Inorg. Chem.* **1999**, *38*, 1671–1682.
[64] F. Studt, F. Tuczek, *Angew. Chem. Int. Ed.* **2005**, *44*, 5639–5642.
[65] R. G. Agarwal, S. C. Coste, B. D. Groff, A. M. Heuer, H. Noh, G. A. Parada, C. F. Wise, E. M. Nichols, J. J. Warren, J. M. Mayer, *Chem. Rev.* **2022**, *122*, 1–49.
[66] J. J. Warren, T. A. Tronic, J. M. Mayer, *Chem. Rev.* **2010**, *110*, 6961–7001.
[67] D. Specklin, A. Coffinet, L. Vendier, I. Del Rosal, C. Dinoi, A. Simonneau, *Inorg. Chem.* **2021**, *60*, 5545–5562.
[68] J. Chatt, R. H. Crabtree, E. A. Jeffery, R. L. Richards, *J. Chem. Soc. Dalton Trans.* **1973**, 1167–1172.

Manuscript received: October 18, 2024
Accepted manuscript online: December 17, 2024
Version of record online: January 13, 2025